On the Role of Protein Disulfide Isomerase in the Retrograde Cell Transport of Secreted Phospholipases A$_2$

Jernej Oberčkal[1]◉, Lidija Kovačič[1]◉, Jernej Šribar[1]◉, Adrijana Leonardi[1], Klemen Dolinar[1], Anja Pucer Janež[1], Igor Križaj[1,2]*

1 Department of Molecular and Biomedical Sciences, Jožef Stefan Institute, Ljubljana, Slovenia,
2 Department of Chemistry and Biochemistry, Faculty of Chemistry and Chemical Technology, University of Ljubljana, Ljubljana, Slovenia

◉ These authors contributed equally to this work.
* igor.krizaj@ijs.si

Abstract

Following the finding that ammodytoxin (Atx), a neurotoxic secreted phospholipase A$_2$ (sPLA$_2$) in snake venom, binds specifically to protein disulfide isomerase (PDI) *in vitro* we show that these proteins also interact in living rat PC12 cells that are able to internalize this group IIA (GIIA) sPLA$_2$. Atx and PDI co-localize in both differentiated and non-differentiated PC12 cells, as shown by fluorescence microscopy. Based on a model of the complex between Atx and yeast PDI (yPDI), a three-dimensional model of the complex between Atx and human PDI (hPDI) was constructed. The Atx binding site on hPDI is situated between domains b and b'. Atx interacts hPDI with an extensive area on its interfacial binding surface. The mammalian GIB, GIIA, GV and GX sPLA$_2$s have the same fold as Atx. The first three sPLA$_2$s have been detected intracellularly but not the last one. The models of their complexes with hPDI were constructed by replacement of Atx with the respective mammalian sPLA$_2$ in the Atx—hPDI complex and molecular docking of the structures. According to the generated models, mammalian GIB, GIIA and GV sPLA$_2$s form complexes with hPDI very similar to that with Atx. The contact area between GX sPLA$_2$ and hPDI is however different from that of the other sPLA$_2$s. Heterologous competition of Atx binding to hPDI with GV and GX sPLA$_2$s confirmed the model-based expectation that GV sPLA$_2$ was a more effective inhibitor than GX sPLA$_2$, thus validating our model. The results suggest a role of hPDI in the (patho)physiology of some snake venom and mammalian sPLA$_2$s by assisting the retrograde transport of these molecules from the cell surface. The sPLA$_2$–hPDI model constitutes a valuable tool to facilitate further insights into this process and into the (patho) physiology of sPLA$_2$s in relation to their action intracellularly.

Introduction

Secreted phospholipases A₂ (sPLA₂s, EC 3.1.1.4) form an assemblage of enzymes secreted by cells that hydrolyse glycerophospholipids to *sn*-2 lysoglycerophospholipids and fatty acids [1]. The fundamental role of these molecules in physiology is reflected in the fact that they have been described from viruses to mammals. Based on their structural characteristics they are classified into eleven groups [2]. In humans there are ten enzymatically active sPLA₂s known, GIB, GIIA, GIIC-F, GIII, GV, GX and GXIIA, and two sPLA₂s apparently without enzymatic activity, GXIIB and otoconin-90/95. Expression patterns of these molecules in mammalian tissues differ, so their functions appear to be non-redundant [3]. Either by enzymatic activity or by binding to soluble or membrane receptors [4] these molecules are implicated in many physiological and pathological settings, such as innate immunity, asthma, atherosclerosis, inflammatory diseases, Alzheimer's disease, neuritogenesis, neurotransmitter release and various forms of cancer [5–8]. Despite intensive research on sPLA₂ pathophysiology, the mechanisms of action of most of the known sPLA₂-associated phenomena are not well understood. It is still widely supposed that sPLA₂s act exclusively extracellularly. However, growing evidence concerning the localization of some types of sPLA₂s inside various cells suggests that they also induce certain cellular processes from inside cells. In compartments other than those leading imported proteins to degradation or *de novo* synthesized proteins to secretion, three mammalian sPLA₂s have been detected, GIB, GIIA and GV sPLA₂. GIB sPLA₂ was found in the nucleus of UIII cells, a stromal cell line derived from normal rat uterus, GIIA in the mitochondria and GV sPLA₂ in the nucleus and cytoplasm of U251 astrocytoma, PC12 and P388D1 macrophage-like cells [9–12].

Snake venoms are a rich source of GI and GII sPLA₂s. These are closely related structurally to mammalian sPLA₂s and thus very useful for studying the function of the latter. Ammodytoxin (Atx), the GIIA sPLA₂ from the nose-horned viper (*Vipera a. ammodytes*) is among the most thoroughly studied snake venom sPLA₂s. This molecule is neurotoxic, acting at the presynaptic side of the neuro-muscular synapse [13]. It is internalized into the cytosol, synaptic vesicles and mitochondria of the motoneuron-like NSC34 cells [14], and into the mammalian motor nerve terminal, where it becomes associated with mitochondria and cytoplasmic vesicles [15]. Specific pathways must exist by which Atx crosses the plasma membrane to enter the cytosol and mitochondria of nerve cells and which are likely to share at least some common characteristics with pathways that mammalian orthologues are using. It is important to answer the question as to how Atx crosses cellular membranes, not only in describing the molecular mechanism of its neurotoxicity but also in shedding more light on the pathophysiological function of some homologous mammalian sPLA₂s.

Several years ago we demonstrated that Atx binds strongly *in vitro* to protein disulfide isomerase (PDI) [16]. PDI is an oxido-reductase, located in the lumen of the endoplasmic reticulum (ER) [17]. We proposed then that it could be implicated in the retrograde trafficking of this toxin in a similar way as revealed in the case of some other protein toxins [18–22]. Besides assisting Atx to move retrogradely from Golgi apparatus to ER, PDI can also help Atx to translocate across the ER membrane. Transport between Golgi apparatus and ER is mediated by cycling of the KDEL receptor. KDEL, or a similar sequence, is located specifically at the C-termini of the ER-resident proteins and prevents them from escaping from the ER lumen. While cholera toxin possesses this signal sequence intrinsically, in its A-subunit, Atx does not but may take advantage of the signal sequence of PDI if complexed with PDI *in vivo*, in the lumen of the ER. The results reported here strongly support the hypothesis that PDI partakes at the retrograde cellular transport of Atx and the related mammalian sPLA₂s. The sPLA₂–

hPDI model that we present provides a structural insight into the interaction between these proteins thus enabling a targeted study of the sPLA$_2$ cell internalization process.

Materials and Methods

Materials

Two isoforms of Atx, AtxA and AtxC, having very similar biological activity [13], were used in our experiments. They were purified from *Vaa* venom as described previously [23]. Sulfo-SBED reagent (sulfosuccinimidyl-2-[6-(biotinamido)-2-(*p*-azidobenzamido)-hexanoamido] ethyl-1,3′-dithio propionate), streptavidin conjugated with horseradish peroxidase (SA—HRP) and monomeric avidin were purchased from Pierce. The fluorogenic substrate PyPG for measuring phospholipase activity was prepared from 1-hexadecanoyl-2-(1-pyrenedecanoyl)-*sn*-glycero-3-phosphoglycerol (Molecular Probes) as described [24]. Bovine α-chymotrypsin, Triton X-100, Tween 20, dithiothreitol (DTT), N-2-hydroxyethylpiperazine-N-2-ethanesulfonic acid (HEPES), glutathione (reduced and oxidized forms) and fatty acid-free bovine serum albumin (BSA) were from Sigma. Human group V and group X sPLA$_2$ (hGV and hGX sPLA$_2$) were produced as described [25]. Recombinant wild type yeast PDI (wt yPDI) and its domains were a gift from Dr. William J. Lennarz, Stony Brook University, New York, USA. These proteins were produced as described [26]. Recombinant human PDI-A1 (hPDI-A1) was from Biorbyt. Rabbit polyclonal anti-PDI IgGs were form Enzo Life Sciences. Mouse polyclonal anti-calmodulin (CaM) IgGs were from Abcam. Protein-A Sepharose was from Amersham Biosciences. BM Chemiluminescence and Lumi-Light^{PLUS} Western Blotting Substrate were from Roche Diagnostics. Other chemicals were obtained mainly from Sigma and Serva and were of at least analytical grade.

PC12 cell culture

PC12 is a cell line derived from a pheochromocytoma of the rat adrenal medulla [27]. PC12 cells ATCC CRL-1721 (American Type Culture Collection, USA) were grown at 37°C under 5% (v/v) CO$_2$ in 10-cm culture plates in F12K (Kaighn's modification of Ham's F-12) growth medium (Gibco, USA) containing 15% (v/v) horse serum, 2.5% (v/v) fetal bovine serum, 100 units/mL of penicillin and 100 μg/mL streptomycin (culture medium). To induce differentiation, nerve growth factor (NGF) was added to the growth medium (100 ng/mL). After 48 hours, the cells were washed with phosphate buffered saline (PBS), fresh NGF-containing growth medium was added, and the cells grown for a further 48 hours. For microscopy, cells were plated on poly-L-Lys coated coverslips and, for viability and mitochondrial membrane potential assays, the cells were plated on 96-well plates.

Testing the influence of Atx on PC12 cells

The influence of Atx on the morphological integrity of non-differentiated (ND) and NGF-differentiated (NGFD) cells was examined. These cells were grown for 120 min at 37°C in the presence of 100 nM AtxC, then inspected for their morphological integrity under a phase contrast microscope Axio Observer Z1 (Carl Zeiss, Germany) using a Plan-Apochromat 40x/0.95 Corr Ph3 M27 objective.

The effect of Atx on the mitochondrial potential of PC12 cells was evaluated. The cells (ND and NGFD), in 96-well plates (10^4 cells per well), were incubated in the dark with 2 μM JC-1 dye (Life Technologies, USA) in F12K growth medium for 20 min at 37°C under 5% (v/v) CO$_2$. After washing with the medium, the cells were incubated in the dark for a further 30 min at 37°C under 5% (v/v) CO$_2$ in the growth medium alone (control) or in the medium

supplemented with either 100 nM AtxA or 50 μM CCCP (mitochondrial uncoupler carbonyl cyanide m-chlorophenyl hydrazone). The green fluorescence of JC-1 at 529 nm and the red fluorescence at 590 nm of aggregated JC-1 were measured in triplicate samples on a SAFIRE microplate reader (Tecan, Austria), using the excitation wavelength 488 nm. The mitochondrial membrane potential was exhibited as the ratio of red to green signals of the cells in the presence of the substance investigated relative to the same ratio in the absence of this substance.

The influence of Atx on the metabolic activity of PC12 cells was measured as follows. PC12 cells (ND and NGFD) in 96-well plates (5×10^4 cells per well) were incubated without (control) or with either 100 nM AtxA or 1% (m/v) Triton X-100 in culture medium at 37°C and 5% (v/v) CO_2. After different incubation times, the cells were washed twice with F12K growth medium and incubated in the dark for a further 2 hours at 37°C under 5% (v/v) CO_2 with MTS (3-(4,5-dimethylthiazol-2-yl)-5-(3-carboxymethoxyphenyl)-2-(4-sulfophenyl)-2H-tetrazolium) (20 μL per 100 μL F12K growth medium) prepared according to the manufacturer's (Promega, USA) instructions. After 2 hours, the absorbance at 490 nm was measured on a SAFIRE microplate reader. The background absorbance was measured on wells containing MTS in F12K growth medium without cells. Viability of cells was calculated from A_{490} corrected for background absorbance and presented relative to the control cells. Measurements were performed in triplicate.

Testing internalization of Atx into PC12 cells

The internalization test used by Jenko Pražnikar et al. [14] was used. In brief, sulfo-SBED-Atx, synthesized as described [28,29], was incubated in the dark with ND and NGFD PC12 cells in culture. Following photo-activation of the Atx probe, cellular proteins in tight complexes with the probe were labelled with biotin. Cells were lysed, the biotinylated proteins selectively extracted using avidin beads and probed for anti-CaM IgG cross-reactivity by Western blotting.

Labelling PDI in PC12 cells with sulfo-SBED-Atx

Intact PC12 cells (both ND and NGFD), plated on 10 cm plates at 80–90% confluence, were treated with sulfo-SBED-Atx at a final concentration of 100 nM for 1, 2, 5, 15, 30 and 60 min in Hank's balanced salt solution supplemented with 1.26 mM Ca^{2+} (Ca^{2+}/HBSS) in the dark at 37°C and 5% (v/v) CO_2. Subsequently, cells were cooled on ice, exposed for 5 min to five 15 W 312 nm UV lamps from a distance of 5 cm, washed twice with Ca^{2+}/HBSS, 1.5% (w/v). Triton X-100/Ca^{2+}/HBSS extracts were then prepared. Experiments were performed in duplicate using cells of the same passage. The extracts were centrifuged for 45 min at $14.000 \times g$ and 4°C. Supernatants were incubated with 375 μL monomeric avidin beads for 1 hour at 4°C. The beads were thoroughly washed with Ca^{2+}/HBSS containing 0.1% (w/v) Triton X-100 and biotin containing proteins then eluted with 2 mM D-biotin. The fractions were concentrated and the proteins recovered as described [30]. The resulting pellets were dissolved in SDS-PAGE loading buffer and analyzed as described below. To standardize the amount of samples applied the intensity of the band corresponding to a protein of 85 kDa (present in control and sulfo-SBED-Atx labelled samples analysed on SDS-PAGE with silver staining) was used as a measure. The position of biotinylated PDI on the gel was determined immunologically using 0.3 μg/mL rabbit polyclonal anti-PDI antibodies.

Immunofluorescence studies

AtxA was dissolved in DMSO (2 mg/mL final concentration) and Alexa Fluor 546 (Molecular Probes Alexa Fluor546 Protein Labelling Kit, Life Technologies, USA) was added to a final protein: dye molar ratio of 1: 1.5 in the presence of 100 mM triethylamine. After 1 h shaking in the

dark at room temperature, taurine was added (5 mM final concentration) and the mixture incubated for a further 30 min. The reaction products were separated on RP-HPLC using an Aquapore BU 300 column (30 mm × 4.6 mm) (PerkinElmer, USA) equilibrated with 5% (v/v) solvent B (90% (v/v) acetonitrile and 0.1% (v/v) trifluoroacetic acid (TFA) in water) in solvent A (0.1% (v/v) TFA in water). After application of the sample, the column was washed with 5 mL of solvent A at a flow rate of 1 mL/min and the bound proteins then eluted with a gradient of solvent B in solvent A from 5% to 20% for 3 min, then from 20% to 60% B for 20 min and finally to 100% B for 3 min. Their absorbance was monitored at 215 nm. As selected by mass spectrometry analysis, the Alexa mono-derivative of AtxA ([546]Alexa-Atx) was further characterized to confirm that its enzymatic activity and ability to bind to CaM do not differ from those of the native toxin.

PC12 cells on poly-L-lysine coated coverslips were incubated at 37°C and 5% (v/v) CO_2 in the presence of 100 nM [546]Alexa-Atx for 1, 2, 5, 15, 30, and 60 min. The cells were first washed three times with Dulbecco's phosphate buffered saline (DPBS) at room temperature and then fixed for 10 min in 4% (w/v) paraformaldehyde in DPBS at room temperature. After fixing, the cells were washed for 5 min with ice-cold DPBS, permeabilized for 5 min with ice-cold 0.1% (w/v) Triton X-100 in DPBS and then incubated at room temperature in blocking solution, containing 0.5% (w/v) fish skin gelatine and 10% (w/v) fetal bovine serum in DPBS. Coverslips were then immersed into primary anti-PDI antibody solution (diluted 1: 300 in blocking solution). After 60 min incubation at room temperature, the cells were rinsed three times for 5 min each in DPBS and then incubated for 60 min at room temperature in secondary antibody solution (Alexa Fluor 488 Goat Anti-Rabbit, diluted 1: 2.000 in blocking solution) and, finally, washed three times 5 min each in DPBS. Excess fluid was removed and the slides mounted using ProLong Gold antifade reagent and left to cure. After 24 hours at room temperature in the dark, the edges of the coverslips were sealed with nail polish and analyzed on an inverted confocal laser scanning microscope (Axio Observer Z1 LSM 710, Carl Zeiss, Germany) with a Plan-Apochromat 63/1.40 oil objective. Fluorophores were excited sequentially using Ar (488 nm) and He-Ne (543 nm) lasers. The emitted light was collected through SP 545 and LP 545 filters. Stacks of fluorescent images were acquired and co-localization of the red and green signal calculated with ImageJ [31] and co-localization plugin JACoP [32]. The signal threshold was determined from autofluorescence of the control cells, and was set at 20% of the maximum signal for both red and green channels. Co-localization was represented by Manders' coefficient, *i.e.* the ratio of the summed intensities of pixels from the green channel, for which the intensity in the red channel is above zero, to the total intensity in the green channel.

Preparation of sulfo-SBED-Atx—yPDI conjugates and their analysis

Equimolar amounts of sulfo-SBED-Atx and wt yPDI or its domains in 75 mM HEPES/HCl, pH 8.2, 150 mM NaCl and 2 mM $CaCl_2$ (labelling buffer) were mixed to give 7 μM concentration of each in a final volume of 50 μL. In competition binding assays, 0.5 μM yPDI or 0.2 μM wt hPDI was incubated with sulfo-SBED-Atx (0.5 μM) in the dark, in the absence or the presence of the following competitors: AtxC (50 μM), GV $sPLA_2$ (18 μM) or GX $sPLA_2$ (13 μM). For mapping the Atx—yPDI interaction surface, the final volume of the reaction mixture was 1 mL. After 60 min incubation at room temperature in the dark, the mixtures were irradiated for 10 min on ice by five 15 W UV lamps at 312 nm from a distance of 5 cm.

Sulfo-SBED-Atx labelled samples were analyzed on SDS-PAGE under reducing conditions. Proteins were transferred from the gel to the PVDF or nitrocellulose membrane by Western blotting in a tank filled with Towbin buffer (25 mM Tris/HCl, 192 mM glycine, 0.1% (w/v) SDS and 20% (v/v) MeOH) for 90 min at 200 mA. On the membrane the biotinylated proteins

were detected by SA—HRP and Lumi—Light^PLUS Western Blotting Substrate or the BM Chemiluminescence Western blotting detection system according to the manufacturer's instructions. Kodak BioMax Light Film was used for light capturing (Sigma—Aldrich).

Isolation and identification of biotinylated peptides

The sulfo-SBED-Atx—yPDI conjugate in 1 mL was cleaved at 37°C with three consecutive additions of 1% (w/w) α-chymotrypsin in 30 min intervals. 10% of the digested reaction mixture was analyzed on a reversed-phase high-pressure liquid chromatography (RP-HPLC) system using a Chrompack C18 (100 × 3.0 mm) column equilibrated with 0.1% (v/v) TFA in water (solvent A). After application of the sample, the column was washed with 5 mL of solvent A at a flow rate of 1 mL/min and the bound peptides then eluted with a gradient of 0% to 60% solvent B (90% (v/v) acetonitrile and 0.1% (v/v) TFA in water) in solvent A in 30 min and then to 100% B in 12 min. Absorbance was monitored at 215 nm. To isolate the biotinylated peptides, 90% of the chymotrypsin-digested sulfo-SBED-Atx—yPDI was added to 150 μL monomeric-avidin beads equilibrated with labelling buffer. The beads were then thoroughly washed with the labelling buffer, followed by a short wash with water. The bound biotinylated peptides were stripped off the beads with 0.1% (v/v) TFA in water and separated on RP-HPLC, using the same protocol as described above for the separation of the 10% of the total digestion reaction mixture. 10% of the material not bound to avidin beads was also analyzed under identical conditions. Isolated biotinylated peptides were N-terminally sequenced by automated Edman degradation on an Applied Biosystems Procise 492A sequencing system.

Modelling the tridimensional structure of the Atx—yPDI complex

All water molecules were removed from the crystal structures of yPDI (PDB ID 2b5e and 3boa [26]) and AtxA (PDB ID 3g8g [33]). Models of the Atx—yPDI complex were generated using two protocols. The rigid-body docking protocol Hex 5.1 [34] (http://www.csd.abdn.ac.uk/hex) was carried out as described [29]. Steric clashes between side-chain atoms were removed by energy minimization (the root mean square gradient for energy conversion was set to 3.0 kcal-/mol/Å) with the Tinker Molecular Modeling Package [35] (http://dasher.wustl.edu/tinker/), using CHARMM27 force field parameters [36]. The high ambiguity-driven docking (HAD-DOCK) protocol has been run as described [37–39]. For HADDOCK trials, the default parameters on the web server version of HADDOCK (http://haddock.science.uu. nl/services/HADDOCK/haddock.php) [39] were used with the setting of passive residues (*i.e.* residues not involved in the interaction) identified from the sequences of the surface exposed biotinylated peptides. Both approaches resulted in two models. In the first model Atx binds to the surface of yPDI at a site between its domains b and b' (bb'-binding site) while, in the second model, it binds between its domains a' and c (a'c-binding site). In this way, the interaction of several other sPLA₂s, structurally similar to Atx, with both yPDI and hPDI was modelled. Coordinates of porcine GIB (pGIB) sPLA₂ (ID 1pir), hGIIA sPLA₂ (ID 1pod), hGX sPLA₂ (ID 1le7) and hPDI (ID 4el1), were obtained from the Protein Data Bank, while the model of hGV sPLA₂ was constructed as described [29]. All water molecules and ions were removed from the three-dimensional (3D) structures. sPLA₂ structures were superimposed on the structure of Atx in the bb' and a'c models of the Atx—yPDI complex. In the same way, the hPDI structure was superimposed on the yPDI structure in the bb'-model of the Atx—yPDI complex. In the thus obtained initial structures, potential active residues (*i.e.* residues constituting the interaction area or being situated not more than 10 Å from it) were identified. Semi-flexible segments were manually defined (each PDI domain represented one segment) while passive residues were defined automatically. The HADDOCK procedure was then performed with other

parameters set to default values. Docking trials of the sPLA₂–yPDI interaction yielded models that differ only slightly in the relative positions of sPLA₂s and yPDI. The models with the lowest non-bonded interaction energy (*i.e.* energy of interactions between atoms that are more than three bonds apart) and similar interaction sites were chosen.

In the case of hPDI, no structural restraints were available. Choice of the best Atx—hPDI model was therefore made based on the similarity of the interaction site with that of the Atx—yPDI model and on lowest non-bonded energy criteria. Models of other sPLA₂–hPDI complexes were then evaluated by comparing them to the chosen Atx—hPDI model. The lowest energy sPLA₂–hPDI models that had interaction sites similar to that of Atx in the hPDI model were chosen. In all cases, excepting that of hGX sPLA₂, the process of choosing the best sPLA₂–hPDI model was very straightforward, since the models with the same interaction site as Atx had the lowest non-bonded energy. For hGX sPLA₂, the respective sPLA₂ in the majority of models was offset significantly relative to Atx. Models in which hGX sPLA₂ exhibited the same interaction site as Atx in the Atx—hPDI complex had significantly higher non-bonded energies; we therefore chose the lowest energy model.

Measurement of phospholipase activity using the fluorogenic substrate PyPG

The phospholipase activity of AtxC, in the presence or the absence of yPDI, was determined as described [40] in 50 mM Tris/HCl, pH 7.4, 50 mM KCl, 1 mM CaCl₂, 0.6% (w/v) fatty acid-free BSA.

Results and Discussion

Atx does not significantly affect the integrity of PC12 cells

Influence of Atx on ND and NGFD PC12 cells was evaluated by measuring its effect on the mitochondrial potential, the metabolic activity and the morphology of the cells. While the mitochondrial potential of the cells was about 40% lower in the presence of 100 nM Atx than in its absence, the MTS test showed increased viability of PC12 cells in the presence of Atx (S1 Fig.). These results are in line with previous findings [41]. As part of the complex influence of sPLA₂s on the cells, they can induce opposing effects, proliferation and apoptosis, in mammalian cells. The morphology of both ND and NGFD PC12 cells was examined, under phase contrast microscopy, following their incubation in the absence and presence of the neurotoxic sPLA₂. No visual changes were observed in either type of PC12 cells in the presence of 100 nM Atx, as compared with control cells grown in the absence of Atx (Fig. 1A). Under these experimental conditions therefore neither proliferation of the cells by Atx nor the negative effect of the sPLA₂ on their mitochondria was dominant enough to be reflected in the modified morphology of the cells.

Atx enters the cytosol of PC12 cells

PC12 cells exhibit properties similar to those of neurons, so they were examined as to whether they constitute an appropriate system for studying the mechanism of internalization of the neurotoxic sPLA₂. A photo-reactive derivative of Atx, sulfo-SBED-Atx, was employed. As was shown previously, this molecule is able to cross the plasma membrane and enter the cytosol of NSC-34 motoneuron cells, but not that of the non-neuronal HEK-293 [14] and Caco-2 cells (unpublished results). Using the same protocol, our results clearly show that sulfo-SBED-Atx is capable of entering very quickly the cytosol of both ND and NGFD PC12 cells when added to the culture medium. Thus, after about 1 min of incubation with NGFD PC12 cells and about 2
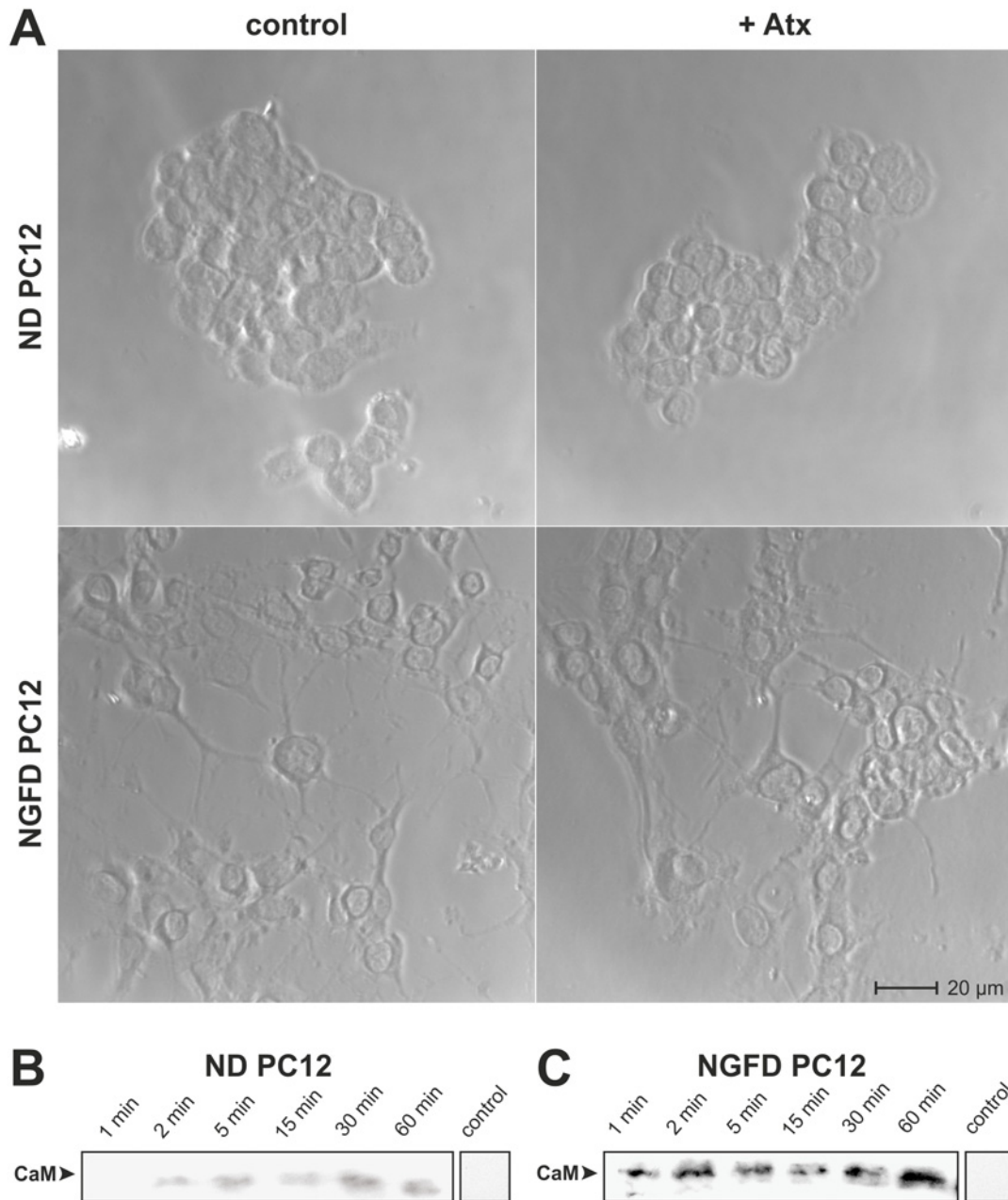
Fig 1. Atx translocates into the cytosol of PC12 cells but does not affect their morphology. (A) Non-differentiated (ND) and NGF-differentiated (NGFD) PC12 cells were incubated with 100 nM AtxC for 120 min at 37°C and then inspected for their morphology under the phase contrast microscope. In control experiments cells were incubated under identical conditions only in the absence of Atx. (B) ND and (C) NGFD PC12 cells were incubated for indicated periods of time with 100 nM sulfo-SBED-Atx in the dark before they were exposed to UV light to trigger photo-cross-linking of the biotin-carrying probe with proteins in close contact. Cells were extracted and biotinylated proteins isolated from extracts on avidin-beads. After reductive SDS-PAGE of biotinylated proteins, these were Western blotted from the gel to a PVDF membrane. The presence of CaM on the PVDF membrane was examined using anti-CaM antibodies and chemiluminescence detection system. Control experiments were performed in an identical way, only without sulfo-SBED-Atx during the 5 min incubation. Experiments were performed in duplicate. Experimental details are given in Materials and Methods.

doi:10.1371/journal.pone.0120692.g001

min with the non-differentiated cells, the photo-reactive probe, tagged its cytosolic high-affinity binding protein CaM with biotin (Figs. 1B and 1C). The degree of labelling of CaM by sulfo-SBED-Atx increased with time of incubation. Similarly rapid internalization of Atx in nerve cells has also been observed with rat hippocampal neurons [42] and with motoneuron-like NSC-34 cells [14]. The fact that Atx is able to enter the cytosol of PC12 cells, apparently without affecting them adversely, qualifies them as suitable for studying the pathway of the neurotoxic sPLA₂ from outside the plasma membrane into the cytosol.

Atx and PDI are significantly co-localized in PC12 cells

The affinity between Atx and PDI has been demonstrated *in vitro* [16]. PDI is a protein in the lumen of the endoplasmic reticulum (ER) known to assist cell invasion by some bacterial toxins such as cholera toxin [18–20]. By analogy, PDI has been proposed as being able to detain and concentrate sPLA₂ molecules in the ER of certain types of cells and to assist them to translocate across the ER membrane into the cytosol [16]. To examine this suggested role of PDI in the (patho)physiology of Atx we first compared the subcellular localization of Atx and PDI in PC12 cells. ND and NGFD cells were incubated in the presence of ^{546}Alexa-Atx (red) for different periods of time, fixed and labelled with anti-PDI antibodies (green) (Figs. 2A and 2B).The distribution of both the red and green signals in the cells was analyzed using confocal laser microscopy, acquiring several optical sections for each sample. Significant red ^{546}Alexa-Atx signal was detected after incubation times of 5 min and longer. It was located on the plasma membrane as well as inside the cells, but absent from the nuclei, at least after up to 120 min of incubation. In all cells, the signal appears discrete. This suggests the localization of Atx in vesicular structures, possibly endosomes. In differentiated PC12 cells, ^{546}Alexa-Atx was distributed in soma and neurites without evident preference, as reported also for the distribution of Atx and β-bungarotoxins, an sPLA₂ neurotoxin from the snake *Bungarus multicinctus*, in rat hippocampal neurons [42,43]. Stacks of images of each sample were quantified and the degree of co-localization of the red and the green signal calculated using ImageJ with co-localization plugin JACoP (Figs. 2C and 2D). To eliminate autofluorescence signals, control experiments without the addition of either ^{546}Alexa-Atx or ^{488}Alexa-conjugated secondary antibodies were used to determine the threshold signal for each channel using Zeiss ZEN Software. The results are represented as the ratio of the number of green pixels that co-localize with red pixels to the total number of green pixels above the threshold. While low co-localization of signals for ^{546}Alexa-Atx and PDI was observed at incubation times up to 5 min, co-localization became significant after 30 min. Based on these results we can conclude that PDI and the neurotoxic sPLA₂ on its way from the external space into the cytosol of the PC12 cell locate regularly at the same sites of the cell.

Atx encounters PDI in living PC12 cells

To further substantiate the suggested role of PDI in the (patho)physiology of some sPLA₂s we investigated the possible formation of the complex between PDI and Atx in living cells. Photo-reactive sulfo-SBED-Atx was added to cultures of ND and NGFD PC12 cells and photo-crosslinking initiated at the incubation times indicated in Figs. 2E and 2F. Cell proteins that were in close contact with Atx at these times remained biotinylated. The cells were then lysed, proteins extracted and loaded to an avidin-affinity column that specifically retained only the biotinylated ones. The avidin-binding proteins were then resolved on SDS-PAGE, electro-blotted onto the PVDF membrane and inspected for the presence of PDI using specific anti-PDI IgGs. As evident from Figs. 2E and 2F, the photoreactive derivative of Atx encountered PDI in both types of PC12 cells. 1 min after the addition of the sPLA₂ to the cell culture
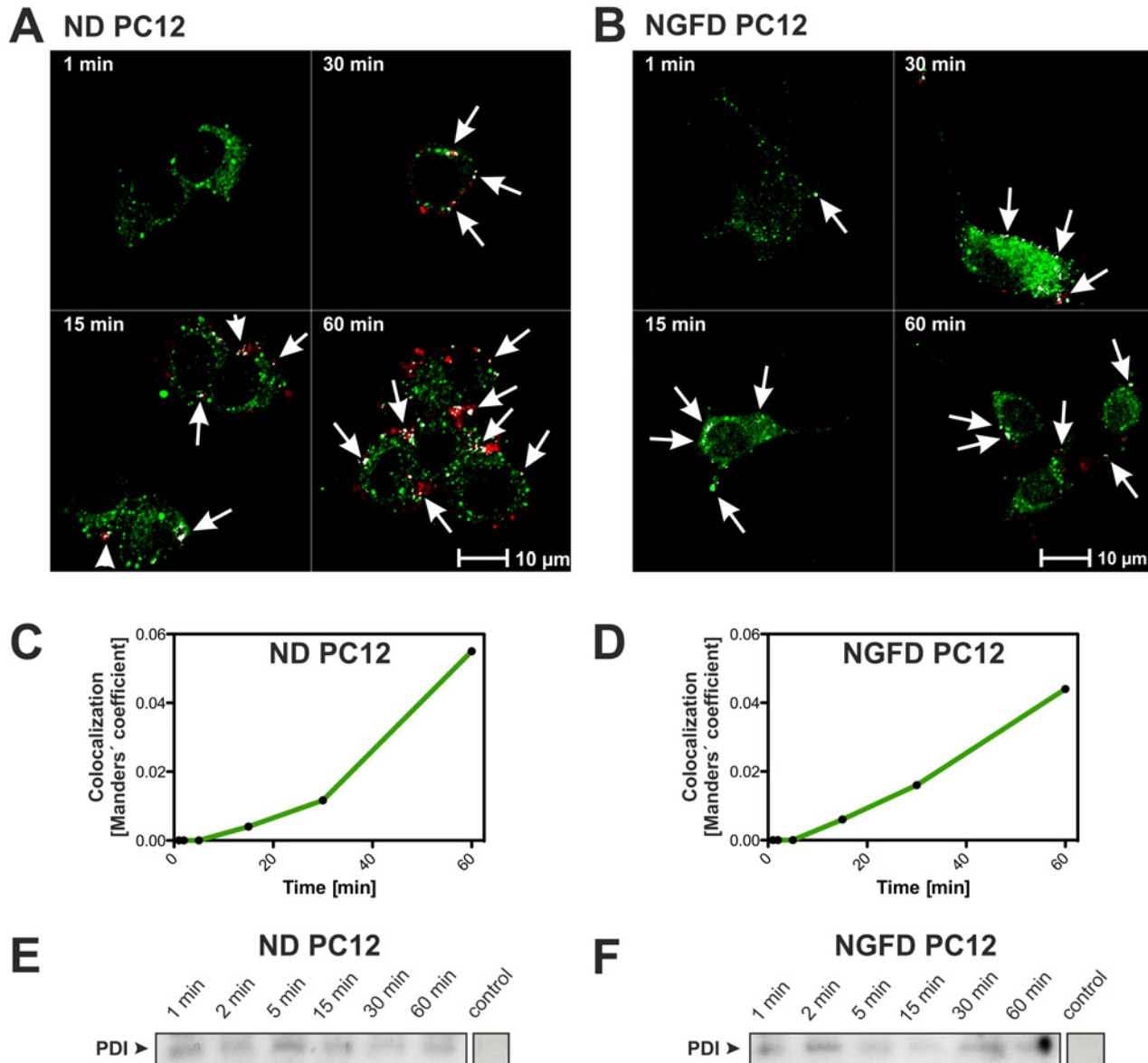
Fig 2. Atx and PDI co-localize and form a complex in living PC12 cells. (A) Non-differentiated (ND) and (B) NGF-differentiated (NGFD) PC12 cells were incubated in the presence of 100 nM ^{546}Alexa-Atx (red signal) for indicated times. Cells were fixed and PDI stained with anti-PDI antibodies (green signal). Co-localized green and red pixels are shown in white. Arrows point at most extensive areas of co-localization. Co-localization of Atx and PDI is expressed in terms of Manders' coefficient in time for ND (C) and NGFD (D) PC12 cells. (E) ND and (F) NGFD PC12 cells were incubated with biotin-containing sulfo-SBED-Atx photo-probe for the indicated time, when this was activated by UV light illumination. The photo-probe covalently links to proteins in close contact, thus biotinylating them. Biotinylated proteins were purified from cell extracts using avidin-affinity chromatography. After reductive SDS-PAGE of biotinylated proteins, these were Western blotted from the gel to a nitrocellulose membrane. The presence of PDI on the membrane was examined using anti-PDI antibodies and chemiluminescence detection system. Control experiments were performed in an identical way, only without sulfo-SBED-Atx during the 5 min incubation. All experiments were performed in duplicate. Experimental details are described in Materials and Methods.

doi:10.1371/journal.pone.0120692.g002

medium it reached the lumen of the ER of the PC12 cells, bound to and reacted with PDI, in agreement with the rapid downstream labelling of the cytosolic CaM (see above). Interestingly, unlike in the case of labelling CaM by sulfo-SBED-Atx (Figs. 1B and 1C), the extent of biotin tagged-PDI did not increase with time. This could indicate that the interaction between Atx and PDI is transient and that the equilibrium between Atx coming into the lumen of ER and

Atx leaving it through the ER membrane into the cytosol is rapidly established. In favour of transient nature of the interaction between Atx and PDI is the apparent dissociation constant of the interaction of 1.27 ± 0.05 µM as determined by surface plasmon resonance [16].

The apparent discrepancy between the results of labelling PDI with sulfo-SBED-Atx, where the product signal remained constant with time, and the result obtained in the co-localization study, where the extent of co-localization increased with time (Figs. 2C and 2D) can be explained by the different nature of the two experiments. In the affinity-labelling experiment only tightly associated molecules of Atx and PDI are observed while, in the co-localization experiment, molecules that are more distant from each other are also indicated. In addition, the methods use differently labelled Atx probes that may have different PDI-binding characteristics. The results, however, strongly support the involvement of PDI in the retrograde cell transport of Atx. A similar function to that of PDI, assistance at moving of sPLA₂ retrogradely from Golgi apparatus to ER, may be also envisaged in the case of two other ER-proteins, TCBP-49 and crocalbin, which bind, respectively, taipoxin and crotoxin, two snake venom neurotoxic sPLA₂s resembling Atx in their action [44,45]. Thus it is concluded that the retrograde cellular transport of sPLA₂s may rely on transient complexing between sPLA₂s and ER-proteins possessing the ER-retaining sequence at their C-termini.

Structural characterization of the interaction between Atx and PDI

In order to design mutants for further study of the role of PDI in cell trafficking of Atx, the interaction between Atx and PDI was characterized in terms of their structures. yPDI was used for three reasons. (1) As hPDI, it binds specifically to Atx (Fig. 3B). (2) It shares substantial homology to hPDI at the levels of the primary, secondary and ternary structure. For example, the orientation of domains b and b', important for enzymatic activity and substrate binding, is very similar in both PDIs. The main difference between the two proteins lies in their C-terminal part—the well-structured α-helix in yPDI (domain c) is absent from hPDI [26,46–48]. (3) In addition, separate recombinant domains of this protein and their fusions were available (Fig. 3A).

In order to locate the Atx-interacting site on yPDI, different parts of the protein—individual domains (a, b, a') and fusions of two or more yPDI domains (a'c, ab, abb', bb'a'c, b'a'c and abb'a') (Fig. 3A)—were reacted with the Atx photo-probe. As evident from Fig. 3C, sulfo-SBED-Atx specifically labelled the following yPDI elements: b, ab, a'c and structures containing these elements, but not domains a and b'. This suggests that two binding sites for sPLA₂ exist on yPDI.

To localize Atx binding sites on yPDI more precisely the interaction area between Atx and yPDI was mapped. To this end, the covalent complex between sulfo-SBED-Atx and yPDI was prepared and fragmented with α-chymotrypsin. The biotin-containing peptides were purified by avidin-affinity chromatography and RP-HPLC (Fig. 4A). The most abundant peptides (peaks 14, 16, 19, 22, 26, 28, 31 and 33 in Fig. 4A) were N-terminally sequenced, enabling their position in the primary structure of Atx or yPDI to be determined (Fig. 4B) and the structural elements in the two proteins that were cross-linked (colour coded in Fig. 4) to be defined. The biotinylated peptides were identified as elements of Atx β-sheet, αE-helix and the C-terminal unstructured area. In the case of yPDI such peptides originated from the bb`- and a`c-region. Identification of peptides clustered in two separate regions of PDI additionally supports the conclusion that yPDI contains two sites to which Atx can bind.
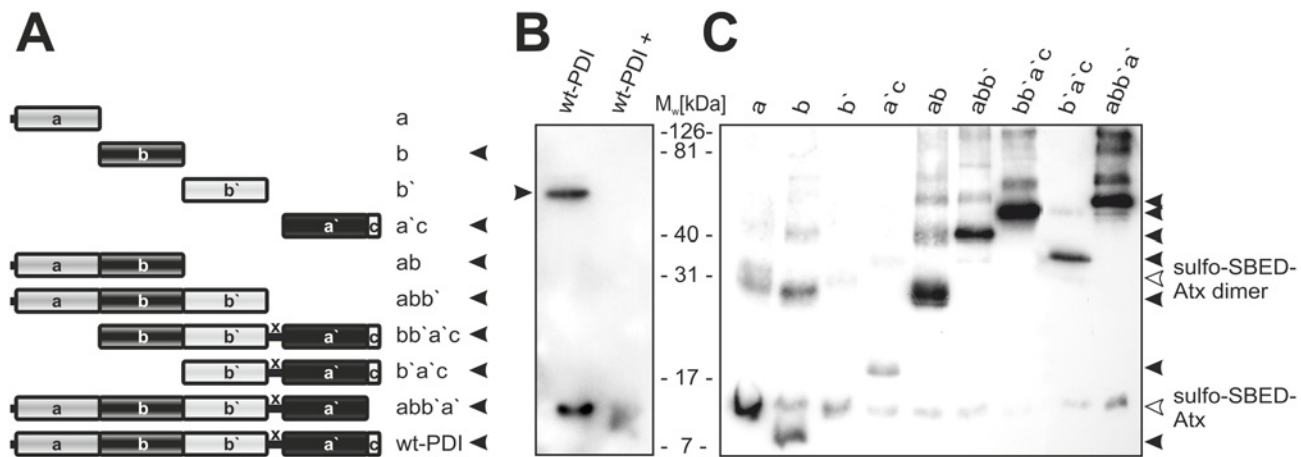
Fig 3. Atx interacts with several domains of yPDI. (A) yPDI is a multi-domain protein. It consists of domains a, a', b, b' and c. Domain b' is linked to domain a' by a linker sequence x. Separate domains and their fusions, as schematically presented, were employed in affinity-labelling experiments using photo-reactive sulfo-SBED-Atx. Atx photo-probe was incubated with the wt yPDI (wt-PDI) (B) or its various parts (C) for 30 min, followed by the UV light-initiated reaction of the photo-probe with proteins in close contact, which were thus biotinylated. Samples were analysed on SDS-PAGE under reducing conditions, electro-transferred to a PVDF membrane. Biotin-containing bands on the PVDF membrane were detected using streptavidin-HRP. Labelling specificity in (B) was verified with the addition of 100-fold unlabelled Atx over sulfo-SBED-Atx (wt-PDI+). Black arrowheads in (A) point at those elements of yPDI which bind and react with sulfo-SBED-Atx. In (B) and (C) black arrowheads are pointing at biotinylated yPDI-structures. Positions on the membrane with biotinylated monomer and dimer of Atx are pointed at by white arrowheads. Experimental details are described in section Materials and Methods. Experiment was performed in triplicate.

doi:10.1371/journal.pone.0120692.g003

Construction of a 3D model of the complex between Atx and yPDI

The structures of Atx and yPDI were docked as described in Materials and Methods, and by considering the structural constraints of the interaction revealed during the binding site mapping experiment. Two alternative docking procedures were employed. In the first, rigid-body docking protocol Hex 5.1 was used. Out of 89 solutions only 2 with the lowest calculated non-bonded energy suited also all of the established structural restraints. Both models were further refined by mild energy minimization allowing only smaller movements of side chain atoms to eliminate steric clashes produced by rigid-body docking. The definition of two final models was confirmed by the high ambiguity-driven docking (HADDOCK) method. Comparison of the two models resulted in only 1.1 Å average backbone Root Mean Square Deviation (RMSD) and, more importantly, in only 0.6 Å average backbone RMSD for the Atx—yPDI interaction surface. In the first model Atx binds to the hydrophobic and acidic surface between domains b and b' of the yPDI (bb'-model). In the second, it binds to the acidic surface at the edge of domain a' of the yPDI that extends to the neighbouring α-helix c (a'c-model) ([Fig. 4C](#)). Modelling thus confirmed the view stemming from affinity labelling and interaction area mapping experiments that Atx can bind at two diverse sites on yPDI.

The details of the interaction between Atx and yPDI at the two binding sites are shown in [Fig. 5](#). The Atx-interacting surface on yPDI in the bb'-model is more extensive than that in the a'c-model. In the latter the electrostatic forces (ionic interactions and hydrogen bonds) between Atx and yPDI are predominant, while in the bb'-model the interaction between Atx and yPDI is supported also by hydrophobic interactions. For this reason it appears that the bb'-binding site is the primary binding site of sPLA₂ on yPDI. The basic R77 and R118 are important amino acid residues in Atx that are involved in binding to the two binding sites on yPDI. In the bb'-model Atx also contacts yPDI with hydrophobic residues, L3, L19 and F24, two polar residues, N17 and N119, and four basic residues, K69, R72, K74 and K86. In the a'c-model Atx interacts with yPDI by two hydrophobic residues, L110 and Y115, a polar N114 and
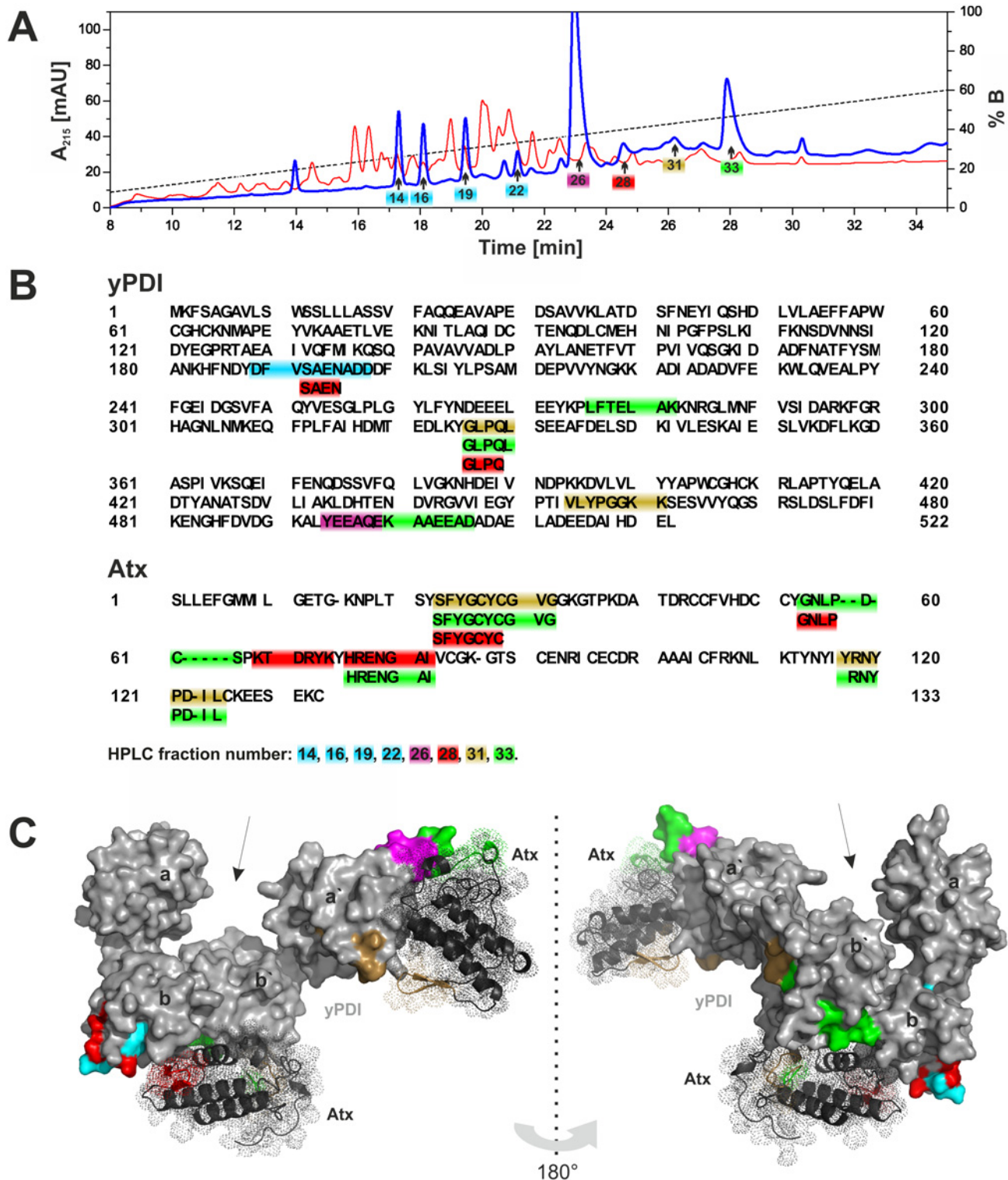
Fig 4. The 3D model of Atx—yPDI complex. (A) Covalent complex of sulfo-SBED-Atx and yPDI was digested with α-chymotrypsin and 10% of the reaction mixture (whole sample) was chromatographed on a Chrompack C18 (100 × 3.0 mm) HPLC column (red line) equilibrated in 0.1% (v/v) TFA and eluted with a gradient of 0.1% (v/v) TFA containing 90% (v/v) acetonitrile. From the rest of the whole sample biotin-containing peptides were isolated on avidin-beads and analysed on HPLC under identical conditions as the whole sample (blue line). Arrows point at fractions containing the major biotinylated peptides. (B) The major biotinylated peptides were identified by N-terminal sequencing. Their positions in primary structures of yPDI or Atx are marked by different colours. A colour designates yPDI and Atx peptides identified in the same fraction. Such peptides are covalently cross-linked and lie close together in the complex, at

the rim of the interaction area between yPDI and Atx. (C) Modelling using rigid-body docking protocol Hex 5.1, HADDOCK procedure and experimentally defined structural restraints resulted in two solutions for Atx binding to yPDI. According to the first, Atx binds to yPDI between domains b and b' (bb'-model or binding site), while according to the second, it binds at domains a' and c of yPDI (a'c-model or binding site). Both solutions are displayed on the same molecule of yPDI using the PyMOL program in two views rotated by 180°. Peptides cross-linked at Atx—yPDI interaction site mapping experiment are indicated by the same colours as in (B). Arrows point towards the active side of yPDI. Experimental details are in Materials and Methods.
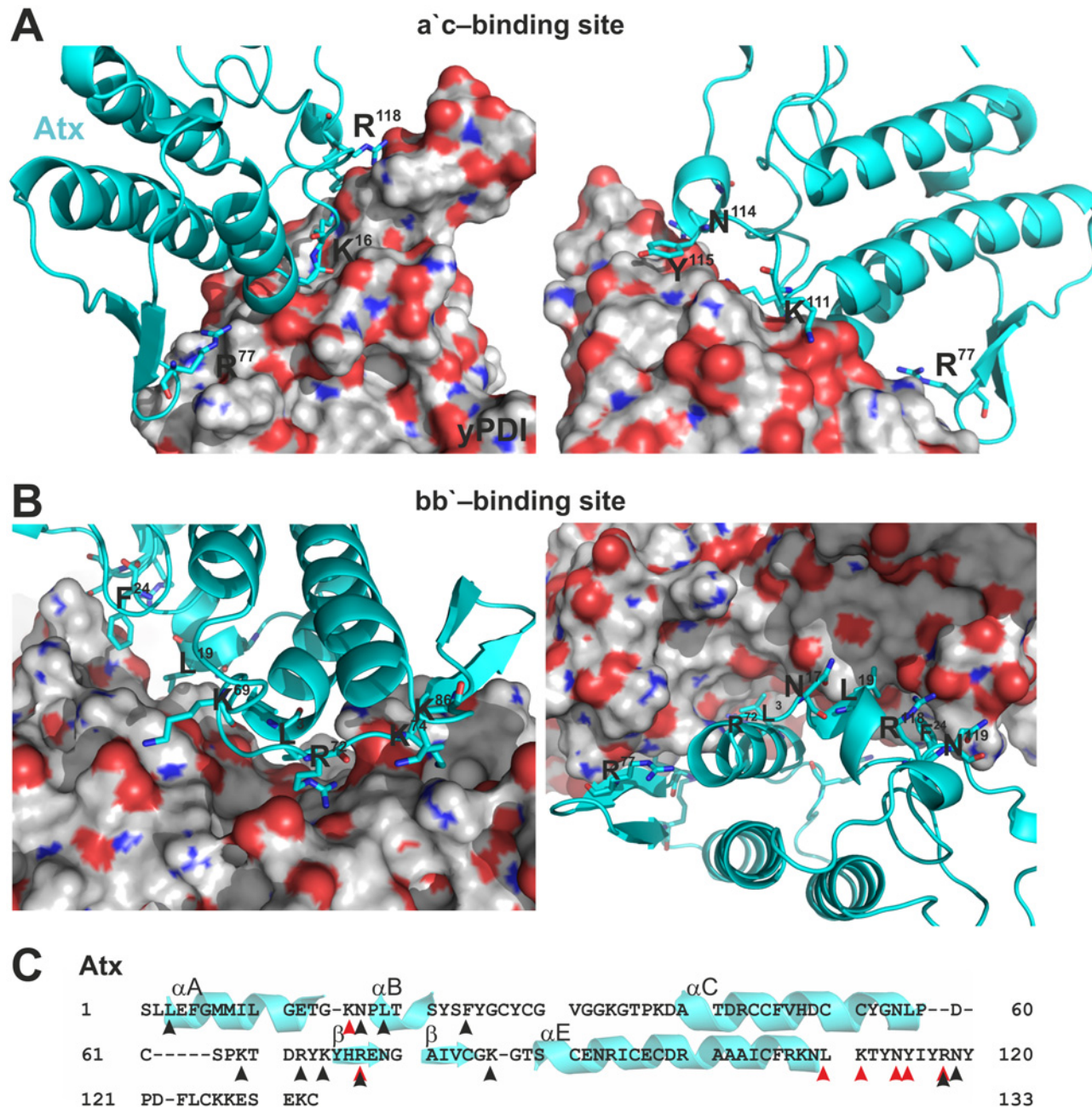
Fig 5. Detailed view of the Atx—yPDI interaction areas. (A) Details of the interaction between Atx and the a'c-binding site of yPDI. (B) Details of the interaction between Atx and the bb'-binding site of yPDI. Structures are prepared using the PyMOL program. yPDI is presented in space-filling mode while Atx in the ribbon mode, with side chains of the yPDI-interacting amino acids shown. (C) The yPDI-contacting amino acid residues of Atx are marked on its primary structure (arrowheads). Black arrowheads point at residues contacting yPDI at the bb'-binding site, while red at those contacting yPDI at the a'c-binding site. Elements of the secondary structure of Atx, α-helices and β-sheets, are shown behind corresponding parts of the primary structure.

two positively charged residues, K16 and K111. Atx faces the bb'-binding site on yPDI with its interfacial binding surface (IBS). Atx binds, with a part of its IBS, to the a'c-binding site on yPDI [49]. Such a mode of binding to PDI should obstruct the binding of Atx to phospholipid membranes, inhibiting its phospholipase activity. However, no influence on the enzymatic activity of Atx has been detected in the presence of PDI. This apparent inconsistency can be explained by the almost 10.000-fold higher affinity of the sPLA₂ molecule for PG membranes than to yPDI [16,50].

Construction of a 3D model of the complex between Atx and hPDI

Human PDIs are heterogeneous with respect to their domain composition. While there are several hPDIs that contain the bb' domain combination, none of them possesses the combination of a'c regions [17]. Our assumption that the bb'-binding site on yPDI is the main sPLA₂-binding site is thus supported from the evolutionary point of view. The bb'-Atx interacting site on yPDI is highly homologous to corresponding regions in the bb'-hPDIs. Misfolded proteins, to be transported back to the cytosol, bind to this region in hPDI [26] as well as cholera toxin [51–53].

The first step in constructing the Atx-hPDI model was to superimpose the 3D structure of hPDI on the structure of yPDI in its bb'-model of the complex with Atx. The HADDOCK procedure was then implemented to obtain the energetically most favourable model of the complex (Fig. 6A). The docking resulted in a structure in which the position of the Atx molecule in the complex is substantially different from that in the complex with yPDI (Fig. 4C). Atx in the complex with hPDI is rotated by 180° and tilted by 5° with respect to its position in the complex with yPDI. Nevertheless, Atx interacts with hPDI *via* its IBS as in the case of yPDI. Interestingly, the same amino acid residues of the sPLA₂, except R77, are involved in ionic, hydrophobic and hydrogen bond interactions with hPDI as with yPDI.

Complexes between PDI and Atx-like mammalian sPLA₂s

Toxins often take advantage of their similarity with endogenous molecules to conquer cells. Several mammalian sPLA₂ molecules, for example GIB, GIIA, GV and GX sPLA₂, are structurally highly homologous to Atx. GIB, GIIA and GV sPLA₂ have been detected inside cells [9–11,54,55] while GX sPLA₂ was not. The pathway of the sPLA₂ cellular internalization has not yet been established. In order to consider the possible involvement of PDI in the cell trafficking of mammalian sPLA₂s, we inspected *in silico* whether the latter are able to form complexes with PDI or not. The 3D structure of each of these molecules was superimposed on the structure of Atx in its complex with PDI. HADDOCK was then used to generate the energetically most favourable models. Besides some differences in relative orientation between respective sPLA₂s in complexes, mammalian sPLA₂s and Atx form very similar complexes with yPDI and hPDI. This is reflected in the average backbone RMSD values calculated for Atx and for each of the replacing sPLA₂s in the complex with PDI. These values for GIB, GIIA, GV or GX sPLA₂ in the case of the yPDI a`c-complex are 4, 3, 3 and 6 Å, respectively. For the yPDI bb'-complex the average backbone RMSD values for GIB, GIIA, GV and GX sPLA₂ are much lower at 0.5, 2, 3 and 1 Å, exposing again the bb'-binding site on the yPDI as the main binding site for sPLA₂s. Average RMSD values for comparison of the backbone atoms of Atx with those of GIB, GIIA, GV and GX sPLA₂ in complex with hPDI are 3, 7, 4 and 12 Å. Consistent with the average RMSD values, GIB, GIIA and GV sPLA₂ form complexes with hPDI similar to the Atx—hPDI complex (Fig. 6B, upper picture), while the interaction area of GX sPLA₂ on hPDI is quite different (Fig. 6B, lower picture), only partially overlapping with those of Atx, GIB, GIIA or GV sPLA₂.
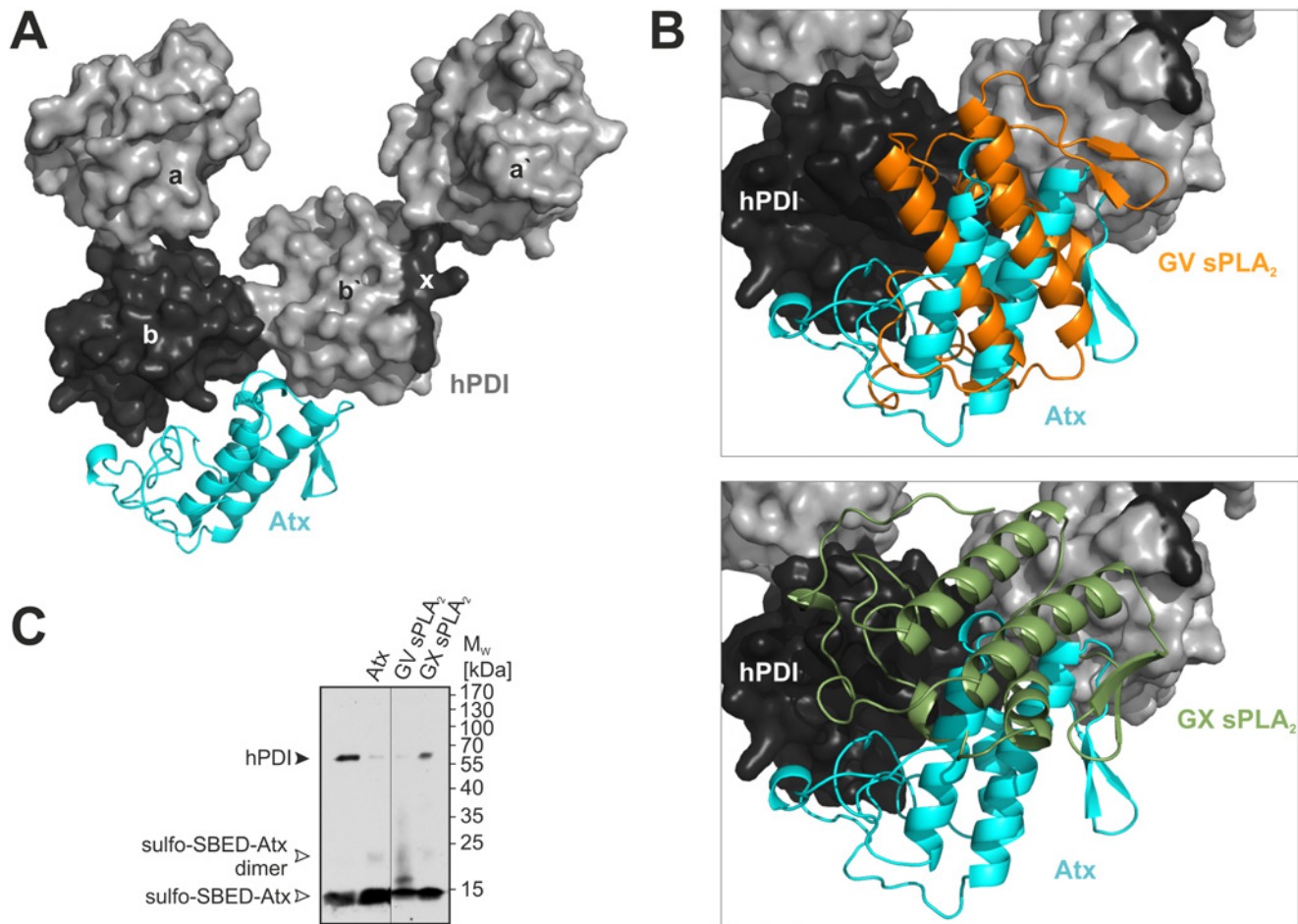
Fig 6. 3D models of complexes between sPLA2s and hPDI. (A) Structure of hPDI was superimposed on the structure of yPDI in the complex with Atx bound to the bb'-binding site and the 3D model optimised by HADDOCK. The model is presented using the PyMOL program with hPDI in space-filling style and Atx in the ribbon style. (B) By substitution of Atx in the Atx—hPDI model with GIB, GIIA, GV or GX sPLA₂, and HADDOCK molecular docking, the models of mammalian sPLA₂s bound to hPDI were generated. GV sPLA₂ (as also GIB and GIIA) occupies the same area on hPDI as Atx (upper picture), while GX sPLA₂ occupies only part of this area (lower picture). (C) Heterologous competition of sulfo-SBED-Atx binding to hPDI by GV and GX sPLA₂s confirms validity of the proposed sPLA₂–hPDI 3D model. Human PDI was incubated with sulfo-SBED-Atx in the dark in the presence of 26 to 100-fold molar excess of AtxC, hGV or hGX sPLA₂ over the sulfo-SBED-Atx. The photo cross-linking reaction was triggered by irradiation at 312 nm. SDS-PAGE analysis under reducing conditions was followed by Western blotting of the samples and biotin-specific detection on the nitrocellulose membranes. Black arrowhead is pointing at the biotinylated hPDI. White arrows are pointing at positions with biotinylated monomer and dimer of Atx. Experimental details are described in Materials and Methods section.

doi:10.1371/journal.pone.0120692.g006

To validate our strategy of modelling the complex between an sPLA₂ and hPDI, we tested experimentally the ability of GV sPLA₂, representative of mammalian sPLA₂s that bind hPDI in the same way as Atx, and GX sPLA₂, the mammalian sPLA₂s that does not bind hPDI in the same way as Atx, to inhibit the binding of sulfo-SBED-Atx on hPDI. From the model we expected that GV sPLA₂ should block biotin-tagging of hPDI more effectively than GX sPLA₂. The results of experimental heterologous competition of sulfo-SBED-Atx binding to hPDI by GV or GX sPLA₂ confirmed our prediction (Fig. 6C). GV sPLA₂ indeed inhibited biotinylation of the hPDI more efficiently than the GX sPLA₂. Our modelling approach thus gives relevant models of complexes between mammalian sPLA₂s and hPDI. Models of the complex between Atx and hPDI, and the Atx-related mammalian sPLA₂s and hPDI thus provide us with a

structural understanding of how these proteins associate. This offers the possibility of facilitating the study of the role of PDI in the sPLA$_2$ cell internalization process by targeted mutagenesis.

Conclusions

The rat PC12 cell line has been shown to be a suitable neuron-like cell model to study the mechanism of the internalization of Atx, the snake venom neurotoxic GIIA sPLA$_2$. Atx does not affect the morphology of these cells but is able to enter their cytosol. We showed that Atx and PDI substantially co-localize in PC12 cells, and, most importantly, are able to form a complex inside living PC12 cells. The results presented here strongly support the proposal that PDI, an oxido-reductase from the lumen of ER, is involved in the retrograde cell transport of Atx. Further study of the role of PDI in cell trafficking of Atx and structurally related mammalian sPLA$_2$s included construction of a 3D model of the complex between Atx and hPDI. Based on this model, the complexes between GIB, GIIA, GV or GX sPLA$_2$, and hPDI were described. These models predict that sPLA$_2$s interact with hPDI in the region including its domains b and b', the same region as that where unfolded proteins and cholera toxin bind on their retrograde pathway to the cytosol. The interaction area with hPDI is the same in the cases of Atx and the mammalian GIB, GIIA and GV sPLA$_2$s, which have been detected intracellularly, while that of GX sPLA$_2$, which has not so far been observed inside cells, is quite diverse in its location. In heterologous competition of Atx binding to hPDI, GV sPLA$_2$ proved to be a better inhibitor than GX sPLA$_2$. The validity of the sPLA$_2$–hPDI 3D model was thus verified experimentally. It qualifies as an important tool to accelerate further insight into the role of PDI in assisting the retrograde transport of certain snake venom and mammalian sPLA$_2$s from the cell surface and into (patho)physiological processes related to the intracellular action of these molecules.

Supporting Information

S1 Fig. The viability of PC12 cells is increased in the presence of Atx. (A) Non-differentiated (ND) and (B) NGF-differentiated (NGFD) PC12 cells were incubated with 100 nM AtxA, in its absence (control) or with 1% (w/v) Triton X-100 for the indicated periods of time. The viability of cells, determined using the MTS viability test, was calculated from A$_{490}$ corrected for background absorbance and is presented relative to the control cells. Experimental details are described in Materials and Methods section.
(TIF)

Acknowledgments

Author Contributions

Conceived and designed the experiments: LK JŠ IK. Performed the experiments: JO LK JŠ AL KD APJ. Analyzed the data: JO LK JŠ AL KD APJ IK. Contributed reagents/materials/analysis tools: LK IK. Wrote the paper: JO LK JŠ AL KD IK.

References

1. Berg OG, Gelb MH, Tsai MD, Jain MK. Interfacial enzymology: the secreted phospholipase A$_2$ paradigm. Chem Rev. 2001; 101: 2613–2654. PMID: 11749391

2. Murakami M, Taketomi Y, Miki Y, Sato H, Hirabayashi T, Yamamoto K. Recent progress in phospholipase A₂ research: from cells to animals to humans. Prog Lipid Res. 2011; 50: 152–192. doi: 10.1016/j.plipres.2010.12.001 PMID: 21185866

3. Eerola LI, Surrel F, Nevalainen TJ, Gelb MH, Lambeau G, Laine VJ. Analysis of expression of secreted phospholipases A₂ in mouse tissues at protein and mRNA levels. Biochim Biophys Acta. 2006; 1761: 745–756. PMID: 16757211

4. Šribar J, Križaj I. Secreted phospholipases A₂—not just enzymes. Acta Chim Slov. 2011; 58: 678–688. PMID: 24061115

5. Murakami M, Taketomi Y, Girard C, Yamamoto K, Lambeau G. Emerging roles of secreted phospholipase A₂ enzymes: lessons from transgenic and knockout mice. Biochimie. 2010; 92: 561–582. doi: 10.1016/j.biochi.2010.03.015 PMID: 20347923

6. Murakami M, Lambeau G. Emerging roles of secreted phospholipase A₂ enzymes: an update. Biochimie. 2013; 95: 43–50. doi: 10.1016/j.biochi.2012.09.007 PMID: 23022039

7. Brglez V, Lambeau G, Petan T. Secreted phospholipases A₂ in cancer: diverse mechanisms of action. Biochimie. 2014; 107: 114–23. doi: 10.1016/j.biochi.2014.09.023 PMID: 25286228

8. Križaj I. Roles of secreted phospholipases A₂ in the mammalian immune system. Protein Pept Lett. 2014; 21: 1201–1208. PMID: 25141938

9. Fayard JM, Tessier C, Pageaux JF, Lagarde M, Laugier C. Nuclear location of PLA₂-I in proliferative cells. J Cell Sci. 1998; 111: 985–994. PMID: 9490642

10. Macchioni L, Corazzi L, Nardicchi V, Mannucci R, Arcuri C, Porcellati S, et al. Rat brain cortex mitochondria release group II secretory phospholipase A₂ under reduced membrane potential. J Biol Chem. 2004; 279: 37860–37869. PMID: 15231825

11. Nardicchi V, Macchioni L, Ferrini M, Goracci G. The presence of a secretory phospholipase A₂ in the nuclei of neuronal and glial cells of rat brain cortex. Biochim Biophys Acta. 2007; 1771: 1345–1352. PMID: 17950028

12. Balboa MA, Shirai Y, Gaietta G, Ellisman MH, Balsinde J, Dennis EA. Localization of group V phospholipase A₂ in caveolin-enriched granules in activated P388D1 macrophage-like cells. J Biol Chem. 2003; 278: 48059–48065. PMID: 12963740

13. Križaj I. Ammodytoxin: a window into understanding presynaptic toxicity of secreted phospholipases A₂ and more. Toxicon. 2011; 58: 219–229. doi: 10.1016/j.toxicon.2011.06.009 PMID: 21726572

14. Jenko Pražnikar Z, Kovačič L, Rowan EG, Romih R, Rusmini P, Poletti A, et al. A presynaptically toxic secreted phospholipase A₂ is internalized into motoneuron-like cells where it is rapidly translocated into the cytosol. Biochim Biophys Acta. 2008; 1783: 1129–1139. doi: 10.1016/j.bbamcr.2008.01.011 PMID: 18261469

15. Logonder U, Jenko-Pražnikar Z, Scott-Davey T, Pungerčar J, Križaj I, Harris JB. Ultrastructural evidence for the uptake of a neurotoxic snake venom phospholipase A₂ into mammalian motor nerve terminals. Exp Neurol. 2009; 219: 591–594. doi: 10.1016/j.expneurol.2009.07.017 PMID: 19631643

16. Šribar J, Anderluh G, Fox JW, Križaj I. Protein disulphide isomerase binds ammodytoxin strongly: possible implications for toxin trafficking. Biochem Biophys Res Commun. 2005; 329: 733–737. PMID: 15737647

17. Appenzeller-Herzog C, Ellgaard L. The human PDI family: versatility packed into a single fold. Biochim Biophys Acta. 2008; 1783: 535–548. PMID: 18093543

18. Tsai B, Ye Y, Rapoport TA. Retro-translocation of proteins from the endoplasmic reticulum into the cytosol. Nat Rev Mol Cell Biol. 2002; 3: 246–255. PMID: 11994744

19. Lencer WI, Tsai B. The intracellular voyage of cholera toxin: going retro. Trends Biochem Sci. 2003; 28: 639–645. PMID: 14659695

20. Lord JM, Roberts LM, Lencer WI. Entry of protein toxins into mammalian cells by crossing the endoplasmic reticulum membrane: co-opting basic mechanisms of endoplasmic reticulum-associated degradation. Curr Top Microbiol Immunol. 2005; 300: 149–168. PMID: 16573240

21. Wernick NLB, Chinnapen DJ-F, Cho JA, Lencer WI. Cholera toxin: an intracellular journey into the cytosol by way of the endoplasmic reticulum. Toxins. 2010; 2: 310–325. doi: 10.3390/toxins2030310 PMID: 22069586

22. Sandvig K, Skotland T, van Deurs B, Klokk TI. Retrograde transport of protein toxins through the Golgi apparatus. Histochem Cell Biol. 2013; 140: 317–326. doi: 10.1007/s00418-013-1111-z PMID: 23765164

23. Gubenšek F, Ritonja A, Zupan J, Turk V. Basic proteins of *Vipera ammodytes* venom—studies of structure and function. Period Biol. 1980; 82: 443–447.

24. Leslie CC, Gelb MH. Assaying phospholipase A₂ activity. Methods Mol Biol. 2004; 284: 229–242. PMID: 15173620

25. Singer AG, Ghomashchi F, Le Calvez C, Bollinger J, Bezzine S, Rouault M, et al. Interfacial kinetic and binding properties of the complete set of human and mouse groups I, II, V, X, and XII secreted phospholipases A₂. J Biol Chem. 2002; 277: 48535–48549. PMID: 12359733

26. Tian G, Xiang S, Noiva R, Lennarz WJ, Schindelin H. The crystal structure of yeast protein disulfide isomerase suggests cooperativity between its active sites. Cell. 2006; 124: 61–73. PMID: 16413482

27. Greene LA, Tischler AS. Establishment of a noradrenergic clonal line of rat adrenal pheochromocytoma cells which respond to nerve growth factor. Proc Natl Acad Sci USA. 1976; 73: 2424–2428. PMID: 1065897

28. Kovačič L, Šribar J, Križaj I. A new photoprobe for studying biological activities of secreted phospholipases A₂. Bioorg Chem. 2007; 35: 295–305. PMID: 17303214

29. Kovačič L, Novinec M, Petan T, Križaj I. Structural basis of the significant calmodulin-induced increase in the enzymatic activity of secreted phospholipases A₂. Protein Eng Des Sel. 2010; 23: 479–487. doi: 10.1093/protein/gzq019 PMID: 20348188

30. Wessel D, Flügge UI. A method for the quantitative recovery of protein in dilute solution in the presence of detergents and lipids. Anal Biochem. 1984; 138: 141–143. PMID: 6731838

31. Schneider CA, Rasband WS, Eliceiri KW. NIH Image to ImageJ: 25 years of image analysis. Nat Methods. 2012; 9: 671–675. PMID: 22930834

32. Bolte S, Cordelières FP. A guided tour into subcellular colocalization analysis in light microscopy. J Microsc. 2006; 224: 213–232. PMID: 17210054

33. Saul FA, Prijatelj-Žnidaršič P, Vulliez-le Normand B, Villette B, Raynal B, Pungerčar J, et al. Comparative structural studies of two natural isoforms of ammodytoxin, phospholipases A₂ from *Vipera ammodytes ammodytes* which differ in neurotoxicity and anticoagulant activity. J Struct Biol. 2010; 169: 360–369. doi: 10.1016/j.jsb.2009.10.010 PMID: 19857576

34. Mustard D, Ritchie DW. Docking essential dynamics eigenstructures. Proteins. 2005; 60: 269–274. PMID: 15981272

35. Ren P, Ponder JW. Polarizable atomic multipole water model for molecular mechanics simulation. J Phys Chem B. 2003; 107: 5933–5947.

36. Foloppe N, MacKerell AD Jr.. All-atom empirical force field for nucleic acids: I. Parameter optimization based on small molecule and condensed phase macromolecular target data. J Comput Chem. 2000; 21: 86–104.

37. Dominguez C, Boelens R, Bonvin AMJJ. HADDOCK: A protein-protein docking approach based on biochemical or biophysical information. J Am Chem Soc. 2003; 125: 1731–1737. PMID: 12580598

38. De Vries SJ, van Dijk M, Bonvin AMJJ. The HADDOCK web server for data-driven biomolecular docking. Nat Protoc. 2010; 5: 883–897. doi: 10.1038/nprot.2010.32 PMID: 20431534

39. Karaca E, Melquiond ASJ, de Vries SJ, Kastritis PL, Bonvin AMJJ. Building macromolecular assemblies by information-driven docking: introducing the HADDOCK multibody docking server. Mol Cell Proteomics. 2010; 9: 1784–1794. doi: 10.1074/mcp.M000051-MCP201 PMID: 20305088

40. Radvanyi F, Jordan L, Russo-Marie F, Bon C. A sensitive and continuous fluorometric assay for phospholipase A₂ using pyrene-labeled phospholipids in the presence of serum albumin. Anal Biochem. 1989; 177: 103–109. PMID: 2742139

41. Petrovič U, Šribar J, Matis M, Anderluh G, Peter-Katalinić J, Križaj I, et al. Ammodytoxin, a secretory phospholipase A₂, inhibits G₂ cell cycle arrest in yeast *Saccharomyces cerevisiae*. Biochem J. 2005; 391: 383–388. PMID: 16008522

42. Petrovič U, Šribar J, Pariš A, Rupnik M, Kržan M, Vardjan N, et al. Ammodytoxin, a neurotoxic secreted phospholipase A₂, can act in the cytosol of the nerve cell. Biochem Biophys Res Commun. 2004; 324: 981–985. PMID: 15485650

43. Herkert M, Shakhman O, Schweins E, Becker CM. Beta-bungarotoxin is a potent inducer of apoptosis in cultured rat neurons by receptor-mediated internalization. Eur J Neurosci. 2001; 14: 821–828. PMID: 11576186

44. Dodds D, Schlimgen AK, Lu SY, Perin MS. Novel reticular calcium binding protein is purified on taipoxin columns. J Neurochem. 1995; 64: 2339–2344. PMID: 7722520

45. Hseu MJ, Yen CY, Tseng CC, Tzeng MC. Purification and partial amino acid sequence of a novel protein of the reticulocalbin family. Biochem Biophys Res Commun. 1997; 239: 18–22. PMID: 9345262

46. Darby NJ, Penka E, Vincentelli R. The multi-domain structure of protein disulfide isomerase is essential for high catalytic efficiency. J Mol Biol. 1998; 276: 239–247. PMID: 9514721

47. Koivunen P, Pirneskoski A, Karvonen P, Ljung J, Helaakoski T, Notbohm H, et al. The acidic C-terminal domain of protein disulfide isomerase is not critical for the enzyme subunit function or for the chaperone or disulfide isomerase activities of the polypeptide. EMBO J. 1999; 18: 65–74. PMID: 9878051

48. Kozlov G, Määttänen P, Thomas DY, Gehring K. A structural overview of the PDI family of proteins. FEBS J. 2010; 277: 3924–3936. doi: 10.1111/j.1742-4658.2010.07793.x PMID: 20796029

49. Petan T, Križaj I, Gelb MH, Pungerčar J. Ammodytoxins, potent presynaptic neurotoxins, are also highly efficient phospholipase A₂ enzymes. Biochemistry. 2005; 44: 12535–12545. PMID: 16156665

50. Šribar J, Čopič A, Pariš A, Sherman NE, Gubenšek F, Fox JW, et al. A high affinity acceptor for phospholipase A₂ with neurotoxic activity is a calmodulin. J Biol Chem. 2001; 276: 12493–12496. PMID: 11278260

51. Forster ML, Mahn JJ, Tsai B. Generating an unfoldase from thioredoxin-like domains. J Biol Chem. 2009; 284: 13045–13056. doi: 10.1074/jbc.M808352200 PMID: 19289469

52. Taylor M, Banerjee T, Navarro-Garcia F, Huerta J, Massey S, Burlingame M, et al. A therapeutic chemical chaperone inhibits cholera intoxication and unfolding/translocation of the cholera toxin A1 subunit. PLoS One. 2011; 6: e18825. doi: 10.1371/journal.pone.0018825 PMID: 21526142

53. Taylor M, Banerjee T, Ray S, Tatulian SA, Teter K. Protein-disulfide isomerase displaces the cholera toxin A1 subunit from the holotoxin without unfolding the A1 subunit. J Biol Chem. 2011; 286: 22090–22100. doi: 10.1074/jbc.M111.237966 PMID: 21543321

54. Kim YJ, Kim KP, Han SK, Munoz NM, Zhu X, Sano H, et al. Group V phospholipase A₂ induces leukotriene biosynthesis in human neutrophils through the activation of group IVA phospholipase A₂. J Biol Chem. 2002; 277: 36479–36488. PMID: 12124392

55. Birts CN, Barton CH, Wilton DC. A catalytically independent physiological function for human acute phase protein group IIA phospholipase A₂: cellular uptake facilitates cell debris removal. J Biol Chem. 2008; 283: 5034–5045. PMID: 18089561